

Opportunistic Wiretapping/Jamming: A New Attack Model in Millimeter-Wave Wireless Networks

Yuanyu Zhang, Zhumeng Zheng, Ji He, Shuangrui Zhao, Qianyue Qu, Yulong Shen, *Member, IEEE*, and Xiaohong Jiang, *Senior Member, IEEE*

Abstract—While the millimeter-wave (mmWave) communication is robust against the conventional wiretapping attack due to its short transmission range and directivity, this paper proposes a new opportunistic wiretapping and jamming (OWJ) attack model in mmWave wireless networks. With OWJ, an eavesdropper can opportunistically conduct wiretapping or jamming to initiate a more hazardous attack based on the instantaneous costs of wiretapping and jamming. We also provide three realizations of the OWJ attack, which are mainly determined by the cost models relevant to distance, path loss and received power, respectively. To understand the impact of the new attack on mmWave network security, we first develop novel approximation techniques to characterize the irregular distributions of wiretappers, jammers and interferers under three OWJ realizations. With the help of the results of node distributions, we then derive analytical expressions for the secrecy transmission capacity to depict the network security performance under OWJ. Finally, we provide extensive numerical results to illustrate the effect of OWJ and to demonstrate that the new attack can more significantly degrade the network security performance than the pure wiretapping or jamming attack.

Index Terms—Physical layer security, millimeter-wave ad hoc networks, wiretapping, jamming.

I. INTRODUCTION

THE past decades have witnessed the explosive growth of wireless devices and the demand for high-speed data traffic, posing a significant challenge to the capacity of wireless communication systems. To address this challenge, both industry and academia have advocated communications over the millimeter-wave (mmWave) bands between 30 and 300 GHz, where the available bandwidths are orders of magnitude greater than conventional sub-6 bands [1]. In addition, the small wavelength of mmWave signals enables large antenna arrays to be deployed in areas as small as a cellphone or even a chip, achieving significantly high antenna gain for both the transmitting and receiving ends [2]. Thanks to the above

Y. Zhang, J. He, S. Zhao and Y. Shen are with the School of Computer Science and Technology, Xidian University, Xi'an, Shaanxi, China and also with Shanxi Key Laboratory of Network and System Security. Y. Zhang is also the Beijing Sunwise Information Technology Ltd, Beijing Institute of Control Engineering, Beijing, China. Email: {yyuzhang, jihe, zhaoshuangrui}@xidian.edu.cn, ylshen@mail.xidian.edu.cn.

Z. Zheng is with the Beijing Sunwise Information Technology Ltd, Beijing Institute of Control Engineering, Beijing, China. Email: zhengzhumeng@sunwiseinfo.com.

Q. Qu is with the Division of Information Science, Graduate School of Science and Technology, Nara Institute of Science and Technology, Ikoma, Nara, Japan, Email: qu.qianyue.q12@is.naist.jp.

X. Jiang is with the School of Systems Information Science, Future University Hakodate, Hakodate, Hokkaido, Japan, and also with the School of Computer Science and Technology, Xidian University, Xi'an, Shaanxi, China. Email: jiang@fun.ac.jp.

benefits, mmWave communication has been regarded as one of the key enabling technologies in future wireless systems like 5G/6G cellular networks [3], unmanned aerial vehicle (UAV) communications [4] and satellite communications [5].

Despite the great potential of mmWave communication, its security issue still has been a critical concern due to the broadcast nature of the wireless medium. Physical layer security techniques have been considered as an important approach to ensuring secure mmWave communication [6]–[10], since they reveal the fundamental capability of achieving information-theoretic and quantifiable security at the physical layer regardless of the computation capabilities of eavesdroppers. Current research on the physical layer security of mmWave communication mainly focuses on combating the conventional wiretapping attack in various mmWave systems, such as mmWave multiple-input and multiple-output (MIMO) systems [11]–[15], mmWave non-orthogonal multiple access (NOMA) systems [16]–[19], intelligent reflecting surface (IRS)-aided mmWave systems [20]–[22], hybrid mmWave-free space optical (FSO) systems [23]–[26] and mmWave ad hoc networks [27]–[29], etc (See Section II for related works).

The aforementioned works help us to understand the impacts of the conventional wiretapping attack on the security performance of mmWave wireless systems, while the recent real-world measurements on mmWave propagation characteristics indicate that mmWave signals are actually less susceptible to the conventional wiretapping attack [30]–[33]. This is mainly due to the following two reasons. First, mmWave signals suffer from severe atmospheric absorption, rain attenuation and penetration loss, leading to a limited transmission range and also the intermittent connectivity of wiretapping links (especially when the links are blocked by obstacles like buildings and human bodies). Second, to combat the severe signal attenuation, transmitters are usually equipped with highly directional antennas with narrow beams, rendering wiretapping on mmWave links much more difficult.

To further identify the potential threats to mmWave communication security, this paper integrates the jamming technique with wiretapping and proposes a more hazardous opportunistic wiretapping and jamming (OWJ) attack model in a mmWave ad hoc network consisting of multiple transmitters, receivers and eavesdroppers distributed according to Poisson Point Processes (PPPs). With OWJ, an eavesdropper can opportunistically conduct wiretapping or jamming based on the instantaneous costs of conducting wiretapping and jamming, aiming at achieving a more significant attack effect. This paper extends its conference version in [34] by adding more OWJ

attack realizations and secrecy performance analysis. The main contributions of this paper are summarized as follows.

- By combining the jamming technique with wiretapping, we propose a new and more hazardous OWJ attack model in mmWave wireless networks, which allows eavesdroppers to conduct wiretapping and jamming opportunistically. This model covers the conventional wiretapping attack and jamming attack as special cases. We also provide three realizations of the OWJ attack, namely distance-related OWJ (DOWJ), loss-related OWJ (LOWJ) and power-related OWJ (POWJ), where the cost of an eavesdropper in wiretapping/jamming is characterized by the distance, path losses and received power, respectively.
- To understand the impact of the OWJ attack on mmWave network security, we first develop novel approximation techniques to characterize the irregular distributions of the wiretappers around a target transmitter, the jammers around a target legitimate receiver and the interferers around a target wiretapper under the three OWJ realizations. With the help of the results of these node distributions, we then derive analytical expressions for the secrecy transmission capacity (STC) to depict the network security performance under the OWJ attack model.
- We finally provide numerical results to illustrate the network STC performance under the OWJ attack model. The results revealed that, in general, the OWJ can more significantly degrade the network security performance than the pure jamming or pure wiretapping attack. In particular, among the three realizations, the POWJ serves as the most hazardous attack, while the DOWJ and LOWJ lead to almost the same attack effect.

The remainder of this paper is organized as follows. We present the related work regarding security performance analysis in mmWave systems under the conventional wiretapping attack in Section II. We introduce the system model in Section III and conduct theoretical performance analysis in Sections IV and V. Section VI presents the numerical results and discussions, and Section VII concludes this paper.

II. RELATED WORK

Existing works on combating the conventional wiretapping attack in mmWave systems mainly focus on the corresponding system security evaluation therein. We categorize these works according to the considered system models as follows.

A. MmWave MIMO Systems

MIMO has been regarded as an appealing technology to reap the benefits of mmWave communication, motivating a plethora of work investigating the security performance of mmWave MIMO systems [11]–[15]. For instance, the joint design of the analog and digital precoders of the secondary transmitter (ST) was investigated to maximize the secrecy rates of the secondary users (SRs) in a mmWave cognitive network with one ST broadcasting information to multiple SRs in the presence of multiple primary users and eavesdroppers [11]. A sparse mmWave massive MIMO network was considered in

[12], where a security scheme was proposed to send information signals through dominant angles of the sparse channel and broadcast AN over the remaining non-dominant angles to interfere only with the eavesdropper. The optimal sparsity parameter was determined to maximize the network secrecy rate. In [13], the secrecy rate was analyzed for a mmWave lens antenna array transmission system and the optimal power allocation between signal and AN was explored to maximize the system secrecy. The optimal beamformer design was investigated for various scenarios, like the downlink communication of mmWave cloud radio access networks (C-RANs) [14] and the dual-polarized mmWave communication systems [15].

B. MmWave NOMA Systems

The combination of the NOMA technology and mmWave communication for enhanced security has recently been a hot research topic [16]–[19]. The authors in [16] considered the downlink transmission in a mmWave NOMA network and proposed a minimal angle-difference user pairing scheme and two maximum ratio transmission beamforming schemes to enhance the network security. In [17], a cognitive mmWave NOMA network was introduced, where each resource block is shared by a user pair consisting of a primary user and a secondary user. The security and reliability performances of the secondary users were investigated under a power allocation scheme that prioritizes the security and QoS requirements of the primary users. The authors in [18] focused on a UAV-to-ground communication scenario, where the UAV base station (BS) adopts the NOMA technology to serve multiple ground users via mmWave downlinks. They proposed a protected-zone approach to suppress the eavesdroppers outside the user region and analyzed the system security performance in terms of the secrecy rate. The NOMA-assisted mmWave UAV downlink scenario was also considered in [19], whereas, different from [18], part of the ground users are energy-constrained and thus use a portion of the power from the BS for energy harvesting and the remaining power for information processing.

C. MmWave IRS Systems

The IRS technology, also known as reconfigurable intelligent surface (RIS), has also been introduced to enhance the security of mmWave communication systems recently [20]–[22]. The authors in [20] considered a mmWave network consisting of BSs, users and RISs, where the locations of BSs and RISs are modeled by homogeneous PPPs. They proposed a two-step association rule to link BSs, users and RISs, and analyzed the area spectrum efficiency and energy efficiency to show the performance gain achieved by the RISs. In [21], an IRS was introduced to assist the BS in securely broadcasting information to users while sending its own information to an IoT device. The precoder at the BS and the beamformer at the IRS were jointly designed to maximize the minimum secrecy rate of multiple users. In [22], the secrecy rate maximization problem was solved for a RIS-aided massive MIMO mmWave downlink scenario with constrained hardware cost and power budget at the transmitter.

D. Hybrid mmWave-FSO Systems

As a promising candidate for backhaul solutions of 5G and beyond 5G networks, hybrid communication systems with mmWave links coexisting with FSO links have attracted considerable attention, and so does the security performance therein [23]–[26]. The authors in [23] conducted security performance analysis in terms of average secrecy capacity, secrecy outage probability and strictly positive secrecy capacity in a parallel FSO-mmWave communication system, where the transmitter sends information to the receiver via an FSO link and a mmWave link concurrently. Three wiretapping scenarios were considered, where the FSO link, mmWave link or both links are wiretapped, respectively. A similar scenario was considered in [24] but with different channel fading randomness, i.e., exponential atmospheric turbulence and Weibull fading channels. The parallel FSO-mmWave system was also considered in [25], while, unlike [23], the authors focused on a wiretapping channel that is correlated to the main channel and hybrid eavesdroppers that can wiretap both the FSO and mmWave links. Apart from the parallel FSO-mmWave system, a serial two-hop FSO-mmWave system consisting of one FSO link and one mmWave link has been introduced in [26], where the average secrecy capacity and secrecy outage probability were analyzed for system security performance analysis.

E. mmWave Ad Hoc Networks

Research efforts have also been devoted to the security performance analysis of mmWave ad hoc networks. The authors in [27] considered a mmWave ad hoc network with transmitters, receivers, potential jammers and eavesdroppers distributed according to PPPs. They proposed a sight-based cooperative jamming scheme, where each potential jammer that has a non-Line-of-Sight (NLoS) link to its nearest receiver but may have LoS links to eavesdroppers is selected with a certain probability to radiate AN such that channel advantages at the receivers can be achieved. The network STC performance was analyzed to show the secrecy gain achieved by the proposed scheme. In [28], a similar scenario without potential jammers was considered and the average achievable secrecy rate was analyzed under a simple AN-based transmission scheme, where each transmitter allocates a fraction of its transmit power to radiate AN. A 3D ad hoc network was considered in [29], where UAVs transmit to ground receivers in the presence of ground eavesdroppers. The secrecy rate performance was investigated under a simple cooperative jamming scheme that allows part of the UAVs to radiate AN without taking their link conditions to the ground receivers into consideration.

III. SYSTEM MODEL

In this section, we introduce the network, antenna, blockage and propagation models, followed by the proposed OWJ attack model and the performance metrics.

A. Network Model

We consider a Poisson bipolar network comprising a set of mmWave transmitter-receiver pairs, where each receiver is

TABLE I
ANTENNA PARAMETERS (ML: MAIN LOBE, SL: SIDE LOBE)

Parameters	Transmitter	Receiver	Wiretapper	Jammer
ML width	θ_T	θ_R	θ_W	θ_J
SL width	$2\pi - \theta_T$	$2\pi - \theta_R$	$2\pi - \theta_W$	$2\pi - \theta_J$
ML gain	G_M^T	G_M^R	G_M^W	G_M^J
SL gain	G_S^T	G_S^R	G_S^W	G_S^J

located at a fixed distance r_0 away from its transmitter but at random orientation. The locations of the transmitters and receivers are modeled by two *dependent* PPPs Φ_T and Φ_R of the same intensity [35], denoted by λ . To simplify the analysis, we neglect the dependence between Φ_T and Φ_R , which still achieves accurate approximations, as can be seen from [27] and the results in this paper. Also present in the network is a set of *half-duplex* eavesdroppers, whose locations are modeled by another independent and homogenous PPP Φ_E of intensity λ_E . Each eavesdropper independently selects to conduct the *wiretapping* attack or the *jamming* attack based on a certain OWJ strategy, as introduced in Section III-D. The resulting wiretappers and jammers form two independent PPPs, denoted by Φ_W and Φ_J , respectively. Using $\mathbf{1}_J^z$ to indicate whether an eavesdropper z is a jammer (i.e., $\mathbf{1}_J^z = 1$) or not (i.e., $\mathbf{1}_J^z = 0$), we have

$$\Phi_J = \{z \in \Phi_E : \mathbf{1}_J^z = 1\}, \Phi_W = \{z \in \Phi_E : \mathbf{1}_J^z = 0\}. \quad (1)$$

B. Antenna Model

Each node is equipped with an antenna array to form a directional antenna. To approximate such antennas, we adopt the sectored antenna model [6]–[10], [27], where each antenna consists of a main lobe and a side lobe. The key antenna parameters of different node types are summarized in Table I. Due to the isotropic feature of the PPPs, the effective antenna gain between a transmitting node a of type $t_1 \in \{T, J\}$ (T : transmitter, J : jammer) and a receiving node b of type $t_2 \in \{R, W\}$ (R : receiver, W : wiretapper) can be represented by the following random variable

$$G_{t_1, t_2}^{a, b} = \begin{cases} G_M^{t_1} G_M^{t_2}, & \text{w.p. } p_{MM}^{t_1 t_2} = \frac{\theta_{t_1} \theta_{t_2}}{(2\pi)^2} \\ G_M^{t_1} G_S^{t_2}, & \text{w.p. } p_{MS}^{t_1 t_2} = \frac{\theta_{t_1} (2\pi - \theta_{t_2})}{(2\pi)^2} \\ G_S^{t_1} G_M^{t_2}, & \text{w.p. } p_{SM}^{t_1 t_2} = \frac{(2\pi - \theta_{t_1}) \theta_{t_2}}{(2\pi)^2} \\ G_S^{t_1} G_S^{t_2}, & \text{w.p. } p_{SS}^{t_1 t_2} = \frac{(2\pi - \theta_{t_1})(2\pi - \theta_{t_2})}{(2\pi)^2} \end{cases}, \quad (2)$$

where w.p. stands for *with probability*. Prior to transmissions, each pair of transmitter and receiver align their antennas to achieve the largest antenna gain $G_M^T G_M^R$.

C. Blockage and Propagation Model

Due to the existence of blockages, communication links can be LoS or NLoS. According to the blockage model in [36], a link of length r is LoS with probability $p_L(r) = e^{-\beta r}$ and NLoS with probability $p_N(r) = 1 - p_L(r)$, where β denotes the blockage density. We use $\mathcal{S}_{a, b}$ to represent the status of the

link $a \rightarrow b$ between nodes a and b . $\mathcal{S}_{a,b} = L$ (resp. $\mathcal{S}_{a,b} = N$) means that the link is LoS (resp. NLoS). Links suffer from both large-scale path loss and small-scale fading characterized by the Nakagami fading model. The path loss of the link $a \rightarrow b$ is $d_{a,b}^\alpha$, where $d_{a,b}$ denotes the distance between nodes a and b , and α is the random path-loss exponent, which equals α_L (resp. α_N) if $\mathcal{S}_{a,b} = L$ (resp. $\mathcal{S}_{i,j} = N$). The corresponding channel gain $h_{a,b}$ follows the gamma distribution with shape N and rate N . Here, $N = N_L$ (resp. $N = N_N$) if $\mathcal{S}_{a,b} = L$ (resp. $\mathcal{S}_{a,b} = N$). Throughout this paper, we assume $\alpha_L < \alpha_N$ and $N_L > N_N$.

D. OWJ Attack Molde

In the OWJ attack, each eavesdropper measures the costs of wiretapping and jamming and conducts the wiretapping attack if

$$\text{cost of wiretapping} < \rho \cdot \text{cost of jamming},$$

and conducts the jamming attack otherwise. The bias factor ρ here represents the preference of the eavesdroppers for the wiretapping attack. The larger the ρ is, the more likely eavesdroppers will wiretap. Note that the OWJ attack covers the pure wiretapping (resp. jamming) attack, as ρ tends to ∞ (resp. 0). In this paper, we consider the following three representations of the costs of a typical eavesdropper $z \in \Phi_E$, giving rise to three different realizations of the OWJ attack, i.e., DOWJ, LOWJ, POWJ, respectively. This is motivated by the fact that eavesdroppers manage to improve their attack effect with all the available network knowledge.

- *Smallest distances:* We use the smallest distances from z to the transmitters and receivers to represent the costs of wiretapping and jamming, which are denoted by $D_T^z = \min_{x \in \Phi_T} d_{x,z}$ (wiretapping) and $D_R^z = \min_{y \in \Phi_R} d_{y,z}$ (jamming), respectively. This applies to the case where only the location information of the transmission pairs is known to the eavesdroppers.
- *Smallest path losses:* We use the smallest path losses from z to the transmitters and receivers as the costs. Formally, the costs are given by $L_T^z = \min_{x \in \Phi_T} d_{x,z}^\alpha$ (wiretapping) and $L_R^z = \min_{y \in \Phi_R} d_{y,z}^\alpha$ (jamming), respectively. This applies to the case where both the locations of the transmission pairs and the link status to the transmission pairs are known to the eavesdroppers.
- *Smallest reciprocals of power:* We use the smallest reciprocal of the power received by z (resp. receivers) from the transmitters (resp. z) as the cost of wiretapping (resp. jamming). The costs are formally given by $P_T^z = \min_{x \in \Phi_T} d_{x,z}^\alpha / (P_T G_{T,W}^{x,z})$ (wiretapping) and $P_R^z = \min_{y \in \Phi_R} d_{y,z}^\alpha / (P_J G_{J,R}^{z,y})$ (jamming), where P_T and P_J denote the transmit power and jamming power of the transmitters and jammers, respectively. This applies to the case where the information of instantaneous antenna gains to the transmitters and receivers is also available.

The three OWJ attack realizations cover scenarios with different network knowledge available to the eavesdroppers. By analyzing the security performance under the attacks, we can identify the knowledge that has a significant impact on the attack effect.

E. Performance Metrics

Transmitters adopt the Wyner encoding scheme [27] for transmissions, where each confidential message is encoded into a codeword that is randomly selected from multiple candidates. Such randomness is used to confuse eavesdroppers. Two code rates are defined in this scheme, i.e., the code rate for the codeword R_t and that for the confidential message R_s . The difference $R_e = R_t - R_s$ reflects the code rate sacrificed for generating the randomness. We assume that R_t , R_s and R_e are fixed throughout this paper.

We adopt the STC metric to model the security performance, which defines the average sum rate of transmissions in perfect secrecy per unit area. Formally, the STC is given by

$$C_s = \lambda p_c p_s R_s, \quad (3)$$

where p_c denotes the connection probability of transmissions (i.e., the probability that receivers can successfully recover the confidential messages), p_s denotes the secrecy probability of transmissions (i.e., the probability that the eavesdroppers fail to decode the confidential messages). We can see from (3) that p_c and p_s are the key parameters for determining the STC. Thus, we focus on the analyses of these two probabilities in the subsequent sections.

IV. CONNECTION PROBABILITY ANALYSIS

In this section, we first derive a unified expression for the connection probability of a typical transmission pair $x_0 \rightarrow y_0$, which involves a key term, i.e., the Laplace transform of the interference at y_0 from the jammers. We then derive this Laplace transform under the DOWJ, LOWJ and POWJ attacks in Sections IV-B, IV-C and IV-D, respectively.

A. Connection Probability

According to the definition, the connection probability is

$$p_c = \mathbb{P}(\log(1 + \text{SINR}_{x_0, y_0}) > R_t), \quad (4)$$

where SINR_{x_0, y_0} is the signal-to-interference-plus-noise ratio (SINR) of y_0 and given by

$$\text{SINR}_{x_0, y_0} = \frac{P_T G_M^T G_M^R h_{x_0, y_0} r_0^{-\alpha}}{I_{y_0}^T + I_{y_0}^J + \sigma^2}. \quad (5)$$

Here, σ^2 is the noise power at y_0 and $I_{y_0}^T$ (resp. $I_{y_0}^J$) denotes the interference at y_0 caused by the transmitters in Φ_T (resp. jammers in Φ_J). Based on (4) and (5), p_c can be derived as follows.

Theorem 1. *The unified connection probability of the typical transmission pair $x_0 \rightarrow y_0$ under the DOWJ, LOWJ and POWJ attacks can be approximated by*

$$p_c \approx \sum_{k \in \{L, N\}} p_k(r_0) \sum_{t=1}^{N_k} \binom{N_k}{t} (-1)^{t+1} e^{-t\mu_k \sigma^2} \prod_{t_1 \in \{T, J\}} \mathcal{L}_{y_0}^{t_1}(t\mu_k), \quad (6)$$

where $\mu_k = N_k(N_k!)^{-1/N_k} (2^{R_t} - 1) r_0^{\alpha k} / (P_T G_M^T G_M^R)$ and $\mathcal{L}_{y_0}^{t_1}(\cdot)$ ($t_1 \in \{T, J\}$) denotes the Laplace transforms of $I_{y_0}^{t_1}$.

Proof: Conditioned on the event that the link $x_0 \rightarrow y_0$ is in status k (i.e., $\mathcal{S}_{x_0, y_0} = k, k \in \{L, N\}$), p_c is given by

$$p_c^k \approx \sum_{t=1}^{N_k} \binom{N_k}{t} (-1)^{t+1} e^{-t\mu_k \sigma^2} \prod_{t_1} \mathcal{L}_{y_0}^{t_1}(t\mu_k), \quad (7)$$

according to Theorem 1 in [27]. Applying the law of total probability in terms of the link status completes the proof. ■

We can see from (6) that the key terms to determine p_c is the Laplace transforms $\mathcal{L}_{y_0}^{t_1}(\cdot)$. Note that $\mathcal{L}_{y_0}^T(\cdot)$ is independent of the OWJ attack model, while $\mathcal{L}_{y_0}^J(\cdot)$ is not. Prior to deriving $\mathcal{L}_{y_0}^T(\cdot)$, we present the following functions for any $k \in \{L, N\}$, $i \in \{M, S\}$, $j \in \{M, S\}$, $t_1 \in \{T, J\}$ and $t_2 \in \{R, W\}$, which will be used extensively in this paper.

$$\Omega_{t_1, t_2}^{k, i, j}(s, r) = p_{ij}^{t_1 t_2} p_k(r) \left(1 - \left(1 + \frac{s P_{t_1} G_i^{t_1} G_j^{t_2}}{N_k r^{\alpha_k}} \right)^{-N_k} \right), \quad (8)$$

$$\Omega_{t_1, t_2}^k(s, r) = \sum_{i, j} \Omega_{t_1, t_2}^{k, i, j}(s, r), \quad (9)$$

$$\Omega_{t_1, t_2}(s, r) = \sum_k \Omega_{t_1, t_2}^k(s, r). \quad (10)$$

Now, we are ready to derive $\mathcal{L}_{y_0}^T(\cdot)$ in the following lemma.

Lemma 1. *The Laplace transform of $I_{y_0}^T$ under the DOWJ, LOWJ and POWJ attacks is*

$$\mathcal{L}_{y_0}^T(s) = \exp \left(-2\pi\lambda \int_0^\infty \Omega_{T, R}(s, r) r dr \right). \quad (11)$$

Proof: According to the definition, we have

$$\begin{aligned} \mathcal{L}_{y_0}^T(s) &= \mathbb{E} \left[e^{-s I_{y_0}^T} \right] \\ &= \mathbb{E} \left[e^{-s \sum_{x \in \Phi_T \setminus \{x_0\}} P_T G_{T, R}^{x, y_0} h_{x, y_0} d_{x, y_0}^{-\alpha}} \right] \\ &= \mathbb{E}_{\Phi_T} \left[\prod_{x \in \Phi_T \setminus \{x_0\}} \mathbb{E}_{G_{T, R}^{x, y_0}, h_{x, y_0}, \alpha} \left[e^{-\frac{s P_T G_{T, R}^{x, y_0} h_{x, y_0}}{d_{x, y_0}^\alpha}} \right] \right] \\ &\stackrel{(a)}{=} \exp \left(-2\pi\lambda \int_0^\infty \left(1 - \mathbb{E} \left[e^{-\frac{s P_T G_{T, R}^{x, y_0} h_{x, y_0}}{r^\alpha}} \right] \right) r dr \right) \\ &= \exp \left(-2\pi\lambda \int_0^\infty \Omega_{T, R}(s, r) r dr \right), \end{aligned} \quad (12)$$

where (a) follows after applying the probability generating functional of PPP [35]. ■

Next, we derive $\mathcal{L}_{y_0}^J(\cdot)$ under the three OWJ attacks in the following subsections, respectively.

B. Derivation of $\mathcal{L}_{y_0}^J(s)$ under DOWJ Attack

Before deriving $\mathcal{L}_{y_0}^J(s)$, we first establish the following lemma for the probability that an eavesdropper z with distance v to y_0 is a jammer (i.e., $\mathbf{1}_J^z = 1$) under the DOWJ attack.

Lemma 2. *The probability that an eavesdropper z with distance v to the typical receiver y_0 is a jammer under the DOWJ attack is*

$$\begin{aligned} \zeta(v) &= \frac{1}{\rho^2 + 1} + \frac{\rho^2}{\rho^2 + 1} e^{-(\rho^2 + 1)\lambda\pi v^2} \bar{F}_{d_{x_0, z}}(c_v) \\ &\quad - \int_{|v-r_0|}^{c_v} \frac{e^{-(1+\frac{1}{\rho^2})\lambda\pi u^2}}{\rho^2 + 1} f_{d_{x_0, z}}(u) du, \end{aligned} \quad (13)$$

where $c_v = \min\{\max\{\rho v, |v - r_0|\}, v + r_0\}$,

$$\bar{F}_{d_{x_0, z}}(u) = 1 - \frac{1}{\pi} \arccos \left(\frac{r_0^2 + v^2 - u^2}{2r_0 v} \right) \quad (14)$$

is the complementary cumulative distribution function (CCDF) of $d_{x_0, z}$ and

$$f_{d_{x_0, z}}(u) = \frac{2u}{\pi \sqrt{4r_0^2 v^2 - (r_0^2 + v^2 - u^2)^2}} \quad (15)$$

is the corresponding probability density function (PDF).

Proof: See Appendix A. ■

Based on Lemma 2, we derive $\mathcal{L}_{y_0}^J(s)$ under the DOWJ attack in the following lemma.

Lemma 3. *The Laplace transform of $I_{y_0}^J$ under the DOWJ attack can be lower bounded by*

$$\mathcal{L}_{y_0}^J(s) \geq \exp \left(-2\pi\lambda_E \int_0^\infty \Omega_{J, R}(s, v) \zeta(v) v dv \right). \quad (16)$$

Proof: First, we have

$$I_{y_0}^J = \sum_{z \in \Phi_E} \mathbf{1}_J^z P_J G_{J, R}^{z, y_0} h_{y_0, z} d_{y_0, z}^{-\alpha}. \quad (17)$$

Hence,

$$\begin{aligned} \mathcal{L}_{y_0}^J(s) &= \mathbb{E}_{I_{y_0}^J} \left[e^{-s I_{y_0}^J} \right] \\ &= \mathbb{E}_{\Phi_T, \Phi_R} \left[\mathbb{E}_{\Phi_E} \left[\prod_{z \in \Phi_E} \mathbb{E}_{h_{y_0, z}, \alpha, G_{J, R}^{z, y_0}} \left[e^{-s \mathbf{1}_J^z \frac{P_J G_{J, R}^{z, y_0} h_{y_0, z}}{d_{y_0, z}^\alpha}} \right] \right] \right] \\ &= \mathbb{E}_{\Phi_T, \Phi_R} \left[\exp \left(-2\pi\lambda_E \int_0^\infty \left(1 - \mathbb{E}_{G_{J, R}^{z, y_0}, h_{y_0, z}, \alpha} \left[e^{-\frac{s \mathbf{1}_J^z P_J G_{J, R}^{z, y_0} h_{y_0, z}}{v^\alpha}} \right] \right) v dv \right) \right]. \end{aligned} \quad (18)$$

Applying the Jensen's inequality yields

$$\begin{aligned}
\mathcal{L}_{y_0}^J(s) &\geq \exp\left(-2\pi\lambda_E \int_0^\infty \left(1 - \mathbb{E}_{\Phi_T, \Phi_R} \left[\mathbb{E}_{G_{J,R}^{z,y_0}, h_{y_0,z}, \alpha} \left[e^{-\frac{s \mathbf{1}_J^z P_J G_{J,R}^{z,y_0} h_{y_0,z}}{v^\alpha}} \right] \right] \right) v dv\right) \\
&= \exp\left(-2\pi\lambda_E \int_0^\infty \left(1 - \mathbb{P}(\mathbf{1}_J^z = 0) - \mathbb{P}(\mathbf{1}_J^z = 1) \mathbb{E}_{G_{J,R}^{z,y_0}, h_{y_0,z}, \alpha} \left[e^{-\frac{s P_J G_{J,R}^{z,y_0} h_{y_0,z}}{v^\alpha}} \right] \right) v dv\right) \\
&= \exp\left(-2\pi\lambda_E \int_0^\infty \mathbb{P}(\mathbf{1}_J^z = 1) \left(1 - \mathbb{E}_{G_{J,R}^{z,y_0}, h_{y_0,z}, \alpha} \left[e^{-\frac{s P_J G_{J,R}^{z,y_0} h_{y_0,z}}{v^\alpha}} \right] \right) v dv\right) \\
&= \exp\left(-2\pi\lambda_E \int_0^\infty \Omega_{J,R}(s, v) \zeta(v) v dv\right). \quad (19)
\end{aligned}$$

C. Derivation of $\mathcal{L}_{y_0}^J(s)$ under LOWJ Attack

Similar to the analysis in Section IV-B, we first establish the following lemma.

Lemma 4. *The probability that an eavesdropper z with distance v and link status $\tau \in \{L, N\}$ to y_0 is a jammer under the LOWJ attack is*

$$\zeta_\tau(v) = \int_{|v-r_0|}^{v+r_0} \sum_{\kappa \in \{L, N\}} \zeta_\kappa^\tau(u, v) p_\kappa(u) f_{d_{x_0, z}}(u) du. \quad (20)$$

where $\zeta_\kappa^\tau(u, v)$ is

$$\zeta_\kappa^\tau(u, v) = \int_0^{\frac{u^{\alpha\kappa}}{\rho}} e^{-(\Lambda(\lambda, \rho w) + \Lambda(\lambda, w))} \Lambda'(\lambda, w) dw \quad (21)$$

for $u^{\alpha\kappa} < \rho v^{\alpha\tau}$ and is

$$\zeta_\kappa^\tau(u, v) = 1 - \rho \int_0^{v^{\alpha\tau}} e^{-(\Lambda(\lambda, \rho w) + \Lambda(\lambda, w))} \Lambda'(\rho w) dw \quad (22)$$

for $u^{\alpha\kappa} \geq \rho v^{\alpha\tau}$, where

$$\begin{aligned}
\Lambda(\lambda, w) &= \lambda\pi w^{\frac{2}{\alpha N}} - \frac{2\pi\lambda}{\beta^2} \left(1 + \beta w^{\frac{1}{\alpha L}}\right) e^{-\beta w^{\frac{1}{\alpha L}}} \\
&\quad + \frac{2\pi\lambda}{\beta^2} \left(1 + \beta w^{\frac{1}{\alpha N}}\right) e^{-\beta w^{\frac{1}{\alpha N}}}, \quad (23)
\end{aligned}$$

and $\Lambda'(\lambda, w)$ is the derivative of $\Lambda(\lambda, w)$.

Proof: See Appendix B. ■

With the help of Lemma 4, we derive the Laplace transform of $I_{y_0}^J$ under the LOWJ attack in the following lemma.

Lemma 5. *The Laplace transform of $I_{y_0}^J$ under the LOWJ attack can be lower bounded by*

$$\mathcal{L}_{y_0}^J(s) \geq \exp\left(-2\pi\lambda_E \int_0^\infty \sum_{\tau \in \{L, N\}} \Omega_{J,R}^\tau(s, v) \zeta_\tau(v) v dv\right), \quad (24)$$

where $\Omega_{J,R}^\tau(s, v)$ can be obtained from (9).

Proof: We divide Φ_E into independent sub-PPPs Φ_E^τ of eavesdroppers with link status $\tau \in \{L, N\}$ to y_0 , i.e., $\Phi_E = \cup_\tau \Phi_E^\tau$. Formally, Φ_E^τ is given by $\Phi_E^\tau = \{z \in \Phi_E : \mathcal{S}_{z, y_0} = \tau\}$. Hence, we have $I_{y_0}^J = \sum_\tau I_{y_0}^{J, \tau}$, where $I_{y_0}^{J, \tau} = \sum_{z \in \Phi_E^\tau} \mathbf{1}_J^z P_J G_{J,R}^{z, y_0} h_{z, y_0}^\tau d_{z, y_0}^{-\alpha_\tau}$, and thus

$$\mathcal{L}_{y_0}^J(s) = \prod_\tau \mathcal{L}_{y_0}^{J, \tau}(s), \quad (25)$$

where $\mathcal{L}_{y_0}^{J, \tau}(s)$ is the Laplace transform of $I_{y_0}^{J, \tau}$. It follows from Lemma 3 that

$$\mathcal{L}_{y_0}^{J, \tau}(s) \geq \exp\left(-2\pi\lambda_E \int_0^\infty \Omega_{J,R}^\tau(s, v) \zeta_\tau(v) v dv\right). \quad (26)$$

Substituting (26) into (25) completes the proof. ■

D. Derivation of $\mathcal{L}_{y_0}^J(s)$ under POWJ Attack

The probability of being a jammer also depends on the effective antenna gain to the receiver y_0 under the POWJ attack and is given by the following lemma.

Lemma 6. *The probability that an eavesdropper z with distance v , link status $\tau \in \{L, N\}$ and effective antenna gain $G_n^J G_o^R$ ($n, o \in \{M, S\}$) to y_0 is a jammer under the POWJ attack can be approximated by*

$$\zeta_{\tau, n, o}(v) \approx \int_{|v-r_0|}^{v+r_0} \sum_{\kappa, l, m} p_{lm}^{TW} \zeta_{\kappa, l, m}^{\tau, n, o}(u, v) p_\kappa(u) f_{d_{x_0, z}}(u) du \quad (27)$$

where $\kappa \in \{L, N\}$, $l \in \{M, S\}$, $m \in \{M, S\}$, $\zeta_{\kappa, l, m}^{\tau, n, o}(u, v)$ is

$$\int_0^{\frac{\eta_1}{\rho}} e^{-(\hat{\Lambda}_1(\lambda, \rho w) + \hat{\Lambda}_2(\lambda, w))} \hat{\Lambda}'_2(\lambda, w) dw \quad (28)$$

for $\eta_1 < \rho \eta_2$ with $\eta_1 = \frac{u^{\alpha\kappa}}{P_T G_l^T G_m^W}$, $\eta_2 = \frac{v^{\alpha\tau}}{P_J G_n^J G_o^R}$, and is

$$1 - \rho \int_0^{\eta_2} e^{-(\hat{\Lambda}_1(\lambda, \rho w) + \hat{\Lambda}_2(\lambda, w))} \hat{\Lambda}'_1(\lambda, \rho w) dw \quad (29)$$

for $\eta_1 \geq \rho \eta_2$, where

$$\hat{\Lambda}_1(\lambda, w) = \sum_{i \in \{M, S\}} \sum_{j \in \{M, S\}} \Lambda(p_{ij}^{TW} \lambda, P_T G_i^T G_j^W w), \quad (30)$$

$$\hat{\Lambda}_2(\lambda, w) = \sum_{i \in \{M, S\}} \sum_{j \in \{M, S\}} \Lambda(p_{ij}^{JR} \lambda, P_J G_i^J G_j^R w), \quad (31)$$

$\hat{\Lambda}'_1(\lambda, w)$ and $\hat{\Lambda}'_2(\lambda, w)$ are the derivatives of $\hat{\Lambda}_1(\lambda, w)$ and $\hat{\Lambda}_2(\lambda, w)$, respectively.

Proof: See Appendix C. ■

Note that the approximation in (27) is due to the fact that we neglect the dependence between $G_{T,W}^{x_0, z}$ and $G_{J,R}^{z, y_0}$. Given the probability $\zeta_{\tau, n, o}(v)$, we derive the Laplace transform of $I_{y_0}^J$ under the POWJ attack as follows.

Lemma 7. *The Laplace transform of $I_{y_0}^J$ under the POWJ attack can be approximated by*

$$\mathcal{L}_{y_0}^J(s) \approx \exp\left(-2\pi\lambda_E \int_0^\infty \sum_{\tau, n, o} \Omega_{J,R}^{\tau, n, o}(s, v) \zeta_{\tau, n, o}(v) v dv\right) \quad (32)$$

where $\Omega_{J,R}^{\tau,n,o}(s,v)$ can be obtained from (8).

Proof: Similar to the proof of Lemma 5, $\mathcal{L}_{y_0}^J(s)$ can be rewritten as

$$\mathcal{L}_{y_0}^J(s) = \prod_{\tau,n,o} \mathcal{L}_{y_0}^{J,\tau,n,o}(s), \quad (33)$$

where $\mathcal{L}_{y_0}^{J,\tau,n,o}(s)$ is the the Laplace transform of the interference caused by the eavesdroppers with link status τ and effective antenna gain $G_n^J G_o^R$ to y_0 . Based on Lemma 3, $\mathcal{L}_{y_0}^{J,\tau,n,o}(s)$ can be given by

$$\mathcal{L}_{y_0}^{J,\tau,n,o}(s) \geq \exp\left(-2\pi\lambda_E \int_0^\infty \Omega_{J,R}^{\tau,n,o}(s,v) \zeta_{\tau,n,o}(v) v dv\right) \quad (34)$$

Substituting (34) into (33) completes the proof. \blacksquare

V. SECRECY PROBABILITY ANALYSIS

In this section, we focus on the typical link $x_0 \rightarrow y_0$ again and derive a unified expression of the secrecy probability. We then analyze the key term involved in the unified expression, i.e., the Laplace transforms of the interference from the concurrent transmitters to any eavesdropper under the DOWJ, LOWJ and POWJ attacks in Sections V-B, V-C and V-D, respectively.

A. Secrecy Probability

The secrecy probability is formulated as

$$p_s = \mathbb{P}\left(\bigcap_{z \in \Phi_W} \{\log(1 + \text{SINR}_{x_0,z}) \leq R_e\}\right), \quad (35)$$

where $\text{SINR}_{x_0,z}$ denotes the SINR of a wiretapper $z \in \Phi_W$. We consider an equivalent formulation of p_s by assuming that all eavesdroppers wiretap on the typical link. Since jammers actually do not wiretap, we remove their impact by setting their interferences to infinity. We divide the PPP Φ_E into sub-PPPs $\Phi_E^{\kappa,l,m}$ of eavesdroppers with link status $\kappa \in \{L, N\}$ and antenna gain $G_l^T G_m^W$ ($l, m \in \{M, S\}$) to x_0 . Hence, p_s can be rewritten as

$$\begin{aligned} p_s &= \prod_{\kappa,l,m} p_s^{\kappa,l,m} \quad (36) \\ &= \prod_{\kappa,l,m} \mathbb{P}\left(\bigcap_{z \in \Phi_E^{\kappa,l,m}} \{\log(1 + \text{SINR}_{x_0,z}^{\kappa,l,m}) \leq R_e\}\right). \end{aligned}$$

We assume that eavesdroppers can eliminate the interference from the jammers. Thus, for any eavesdropper $z \in \Phi_E^{\kappa,l,m}$, we have

$$\text{SINR}_{x_0,z}^{\kappa,l,m} = \frac{P_T G_{T,W}^{x_0,z} h_{x_0,z} d_{x_0,z}^{-\alpha}}{\hat{I}_z^T + \sigma^2}, \quad (37)$$

where

$$\hat{I}_z^T = \begin{cases} I_z^T, & \mathbf{1}_z = 0 \\ \infty, & \mathbf{1}_z = 1 \end{cases} \quad (38)$$

denotes the interference from concurrent transmitters. Here, $I_z^T = \sum_{x \in \Phi_T \setminus \{x_0\}} P_T G_{T,W}^{x,z} h_{x,z} d_{x,z}^{-\alpha}$. We now derive the secrecy probability based on the above formulations.

Theorem 2. *The secrecy probability of the typical transmission pair $x_0 \rightarrow y_0$ under the DOWJ, LOWJ and POWJ attacks can be approximated by*

$$p_s \approx \exp\left(-2\pi\lambda_E \sum_{\kappa,l,m} p_{lm}^{TW} \sum_{t=1}^{N_\kappa} \binom{N_\kappa}{t} (-1)^{t+1} \int_0^\infty p_\kappa(u) e^{-t\nu_{\kappa,l,m} u^{\alpha_\kappa} \sigma^2} \mathcal{L}_{z,\kappa,l,m}^T(t\nu_{\kappa,l,m} u^{\alpha_\kappa}, u) u du\right), \quad (39)$$

where $\nu_{\kappa,l,m} = \frac{N_\kappa (N_\kappa!)^{-1/N_\kappa} (2^{R_e} - 1)}{P_T G_l^T G_m^W}$ and $\mathcal{L}_{z,\kappa,l,m}^T(\cdot, u)$ denotes the Laplace transform of \hat{I}_z^T for any eavesdropper $z \in \Phi_E^{\kappa,l,m}$ with $d_{x_0,z} = u$.

Proof: According to (36), we first derive $p_s^{\kappa,l,m}$, which is given by

$$\begin{aligned} p_s^{\kappa,l,m} &= \mathbb{P}\left(\bigcap_{z \in \Phi_E^{\kappa,l,m}} \{\log(1 + \text{SINR}_{x_0,z}^{\kappa,l,m}) \leq R_e\}\right) \quad (40) \\ &\approx \exp\left(-2\pi p_{lm}^{TW} \lambda_E \sum_{t=1}^{N_\kappa} \binom{N_\kappa}{t} (-1)^{t+1} \int_0^\infty p_\kappa(u) e^{-t\nu_{\kappa,l,m} u^{\alpha_\kappa} \sigma^2} \mathcal{L}_{z,\kappa,l,m}^T(t\nu_{\kappa,l,m} u^{\alpha_\kappa}, u) u du\right), \end{aligned}$$

following from Theorem 2 in [27]. Substituting (40) into (36) completes the proof. \blacksquare

From (39), we know that the key term involved in p_s is the Laplace transform $\mathcal{L}_{z,\kappa,l,m}^T(s, u)$. In what follows, we will derive the expressions of $\mathcal{L}_{z,\kappa,l,m}^T(s, u)$ under the DOWJ, LOWJ and POWJ attacks, respectively. Prior to the derivation, we first give the following functions for any $k \in \{L, N\}$, $i \in \{M, S\}$, $j \in \{M, S\}$, $t_1 \in \{T, J\}$ and $t_2 \in \{R, W\}$.

$$\Xi_{t_1,t_2}^{k,i,j}(s, \lambda, c) = \exp\left(-2\pi\lambda \int_c^\infty \Omega_{t_1,t_2}^{k,i,j}(s, r) r dr\right), \quad (41)$$

$$\begin{aligned} \Xi_{t_1,t_2}^k(s, \lambda, c) &= \prod_{i,j} \Xi_{t_1,t_2}^{k,i,j}(s, \lambda, c) \\ &= \exp\left(-2\pi\lambda \int_c^\infty \Omega_{t_1,t_2}^k(s, r) r dr\right), \quad (42) \end{aligned}$$

$$\begin{aligned} \Xi_{t_1,t_2}(s, \lambda, c) &= \prod_k \Xi_{t_1,t_2}^k(s, \lambda, c) \\ &= \exp\left(-2\pi\lambda \int_c^\infty \Omega_{t_1,t_2}(s, r) r dr\right), \quad (43) \end{aligned}$$

where $\Omega_{t_1,t_2}^{k,i,j}(s, r)$, $\Omega_{t_1,t_2}^k(s, r)$ and $\Omega_{t_1,t_2}(s, r)$ are given in (8), (9) and (10), respectively.

B. Derivation of $\mathcal{L}_{z,\kappa,l,m}^T(s, u)$ under DOWJ attack

We can see from Section III-D that the DOWJ attack is dependent solely on the distances from z to the transmitters and receivers, which means that the Laplace transform $\mathcal{L}_{z,\kappa,l,m}^T(s, u)$ varies with only $d_{x_0,z} = u$. Thus, we rewrite $\mathcal{L}_{z,\kappa,l,m}^T(s, u)$ as $\mathcal{L}_z^T(s, u)$ under the DOWJ attack, whose expression can be given in the following lemma.

Lemma 8. *The Laplace transform of the interference caused by the concurrent transmitters at any eavesdropper $z \in \Phi_E^{\kappa,l,m}$ with distance u to the typical transmitter x_0 under the DOWJ attack is given by*

$$\begin{aligned} \mathcal{L}_z^T(s, u) &= \Xi_{T,W}(s, \lambda, 0) - \bar{F}_{d_{y_0,z}}(c_u) \\ &\times \int_0^{u/\rho} \Xi_{T,W}(s, \lambda, \rho w) 2\pi \lambda w e^{-(\rho^2+1)\lambda\pi w^2} dw \\ &- \int_{|u-r_0|}^{c_u} \Xi_{T,W}(s, \lambda, \rho v) e^{-(\rho^2+1)\lambda\pi v^2} f_{d_{y_0,z}}(v) dv \\ &- \int_{|u-r_0|}^{c_u} \int_0^v \Xi_{T,W}(s, \lambda, \rho w) \\ &\quad 2\pi \lambda w e^{-(\rho^2+1)\lambda\pi w^2} f_{d_{y_0,z}}(v) dw dv, \end{aligned} \quad (44)$$

where $c_u = \min\{\max\{\frac{u}{\rho}, |u - r_0|\}, u + r_0\}$,

$$\bar{F}_{d_{y_0,z}}(v) = 1 - \frac{1}{\pi} \arccos\left(\frac{r_0^2 + u^2 - v^2}{2r_0u}\right) \quad (45)$$

is the CCDF of $d_{y_0,z}$ and

$$f_{d_{y_0,z}}(v) = \frac{2v}{\pi \sqrt{4r_0^2 u^2 - (r_0^2 + u^2 - v^2)^2}} \quad (46)$$

is the corresponding PDF.

Proof: See Appendix D. ■

C. Derivation of $\mathcal{L}_{z,\kappa,l,m}^T(s, u)$ under LOWJ attack

The LOWJ attack depends on both the distances and link status from z to the transmitters and receivers. Thus, the Laplace transform $\mathcal{L}_{z,\kappa,l,m}^T(s, u)$ under the LOWJ attack varies with both $d_{x_0,z} = u$ and $\mathcal{S}_{x_0,z} = \kappa$. Rewriting $\mathcal{L}_{z,\kappa,l,m}^T(s, u)$ as $\mathcal{L}_{z,\kappa}^T(s, u)$, we give the Laplace transform $\mathcal{L}_{z,\kappa}^T(s, u)$ in the following lemma.

Lemma 9. *The Laplace transform of the interference caused by the concurrent transmitters at any eavesdropper $z \in \Phi_E^{\kappa,l,m}$ with distance u and link status κ to the typical transmitter x_0 under the LOWJ attack is*

$$\mathcal{L}_{z,\kappa}^T(s, u) = \int_{|u-r_0|}^{u+r_0} \sum_{\tau} \mathcal{L}_{z,\kappa}^{T,\tau}(s, u, v) p_{\tau}(v) f_{d_{y_0,z}}(v) dv, \quad (49)$$

where $\mathcal{L}_{z,\kappa}^{T,\tau}(s, u, v)$ is given by (47).

Proof: See Appendix E. ■

D. Derivation of $\mathcal{L}_{z,\kappa,l,m}^T(s, u)$ under POWJ attack

Note that the Laplace transform $\mathcal{L}_{z,\kappa,l,m}^T(s, u)$ under the POWJ attack varies with $d_{x_0,z} = u$, $\mathcal{S}_{x_0,z} = \kappa$ and $G_{T,W}^{x_0,z} = G_l^T G_m^W$. The following lemma summarizes the Laplace transform $\mathcal{L}_{z,\kappa,l,m}^T(s, u)$ under the POWJ attack.

Lemma 10. *The Laplace transform of the interference caused by the concurrent transmitters at any eavesdropper $z \in \Phi_E^{\kappa,l,m}$ with distance u , link status κ and antenna gain $G_l^T G_m^W$ to*

the typical transmitter x_0 under the POWJ attack can be approximated by

$$\mathcal{L}_{z,\kappa,l,m}^T(s, u) \approx \int_{|u-r_0|}^{u+r_0} \sum_{\tau,n,o} p_{no}^{JR} \mathcal{L}_{z,\kappa,l,m}^{T,\tau,n,o}(s, u, v) p_{\tau}(v) f_{d_{y_0,z}}(v) dv, \quad (50)$$

where $\mathcal{L}_{z,\kappa,l,m}^{T,\tau,n,o}(s, u, v)$ is given by (48).

Proof: See Appendix F. ■

VI. NUMERICAL RESULTS

In this section, we provide simulation results to validate the derived secrecy and connection probabilities, followed by discussions on the impacts of system parameters on the STC performance. We also compare the attack effect of the three OWJ attacks in terms of the STC performance.

TABLE II
PARAMETERS USED IN SIMULATIONS.

Parameters	Value
Carrier frequency	28 GHz
Link distance r_0	50m
Channel bandwidth	1 GHz
Noise spectral density	-174 dBm/Hz
Transmit power P_T	1 W (i.e., 30 dBm)
Path loss exponent α_L (α_N)	2 (4)
Nakagami fading parameter N_L (N_N)	3 (2)
Block density β	1/141.4
ML beam width $\theta_T, \theta_R, \theta_J, \theta_W$	$\pi/6$
ML gain $G_M^T, G_M^R, G_M^E, G_M^J$	10
SL gain $G_S^T, G_S^R, G_S^E, G_S^J$	0.1

A. Simulation and Validation

A dedicated simulator was developed to simulate the transmission process in a Poisson mmWave bipolar network. Using this simulator, we conducted simulations for the secrecy probability and connection probability of the network under the DOWJ, LOWJ and POWJ attacks for the settings of $\lambda = 0.0001 \text{ m}^{-2}$, $\lambda_E = 0.0001 \text{ m}^{-2}$, $P_J = 10 \text{ W}$, $R_t = 4 \text{ bps/Hz}$ and $R_e = 2 \text{ bps/Hz}$. The other parameters are summarized in Table II.

We summarize the simulation results and also the theoretical ones in Figs. 1 and 2. We can see from the figures that the theoretical results provide good approximations or tight bounds for the secrecy probability and connection probability under all three OWJ attacks, implying the effectiveness of the derived analytical expressions. We can also see from the figures that, as the bias factor ρ (i.e., the preference for the wiretapping attack) increases, the secrecy probability decreases while the connection probability increases under all three attacks. This is intuitive since a larger ρ leads to more wiretappers and thus fewer jammers in the network.

$$\mathcal{L}_{z,\kappa}^{T,\tau}(s, u, v) = \begin{cases} \Xi_{T,W}(s, \lambda, 0) - \int_0^{\frac{u^{\alpha_\kappa}}{\rho}} e^{-(\Lambda(\lambda, \rho w) + \Lambda(\lambda, w))} \Lambda'(\lambda, w) \prod_{k \in \{L, N\}} \Xi_{T,W}^k \left(s, \lambda, (\rho w)^{\frac{1}{\alpha_k}} \right) dw, & u^{\alpha_\kappa} < \rho v^{\alpha_\tau} \\ \Xi_{T,W}(s, \lambda, 0) - e^{-(\Lambda(\lambda, \rho v^{\alpha_\tau}) + \Lambda(\lambda, v^{\alpha_\tau}))} \prod_{k \in \{L, N\}} \Xi_{T,W}^k \left(s, \lambda, (\rho v^{\alpha_\tau})^{\frac{1}{\alpha_k}} \right) & \\ - \int_0^{v^{\alpha_\tau}} e^{-(\Lambda(\lambda, \rho w) + \Lambda(\lambda, w))} \Lambda'(\lambda, w) \prod_{k \in \{L, N\}} \Xi_{T,W}^k \left(s, \lambda, (\rho w)^{\frac{1}{\alpha_k}} \right) dw, & u^{\alpha_\kappa} \geq \rho v^{\alpha_\tau} \end{cases} \quad (47)$$

$$\mathcal{L}_{z,\kappa,l,m}^{T,\tau,n,o}(s, u, v) \approx \begin{cases} \Xi_{T,W}(s, \lambda, 0) - \int_0^{\frac{\eta_1}{\rho}} e^{-(\hat{\Lambda}_1(\lambda, \rho w) + \hat{\Lambda}_2(\lambda, w))} \hat{\Lambda}'_2(\lambda, w) \prod_{k,i,j} \Xi_{T,W}^{k,i,j} \left(s, \lambda, (\rho w P_T G_i^T G_j^W)^{\frac{1}{\alpha_k}} \right) dw, & \eta_1 < \rho \eta_2 \\ \Xi_{T,W}(s, \lambda, 0) - e^{-(\hat{\Lambda}_1(\lambda, \rho \eta_2) + \hat{\Lambda}_2(\lambda, \eta_2))} \prod_{k,i,j} \Xi_{T,W}^{k,i,j} \left(s, \lambda, (\rho \eta_2 P_T G_i^T G_j^W)^{\frac{1}{\alpha_k}} \right) & \\ - \int_0^{\eta_2} e^{-(\hat{\Lambda}_1(\lambda, \rho w) + \hat{\Lambda}_2(\lambda, w))} \hat{\Lambda}'_2(\lambda, w) \prod_{k,i,j} \Xi_{T,W}^{k,i,j} \left(s, \lambda, (\rho w P_T G_i^T G_j^W)^{\frac{1}{\alpha_k}} \right) dw, & \eta_1 \geq \rho \eta_2 \end{cases} \quad (48)$$

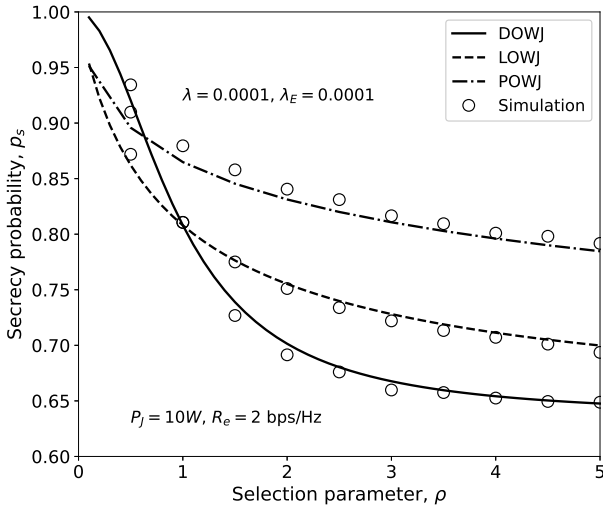


Fig. 1. Secrecy probability vs. bias factor ρ .

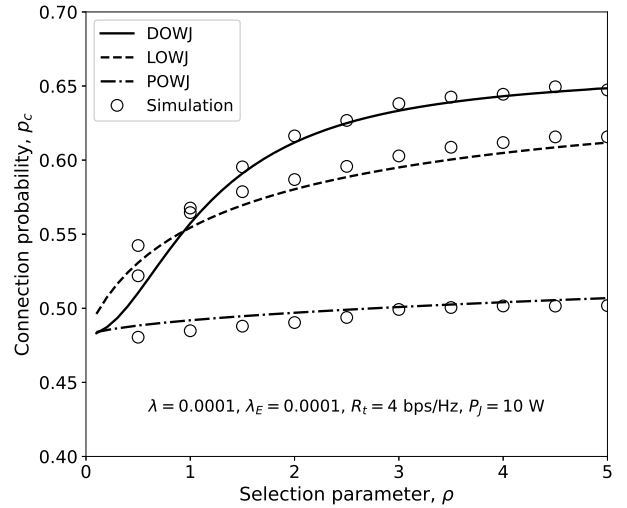


Fig. 2. Connection probability vs. bias factor ρ .

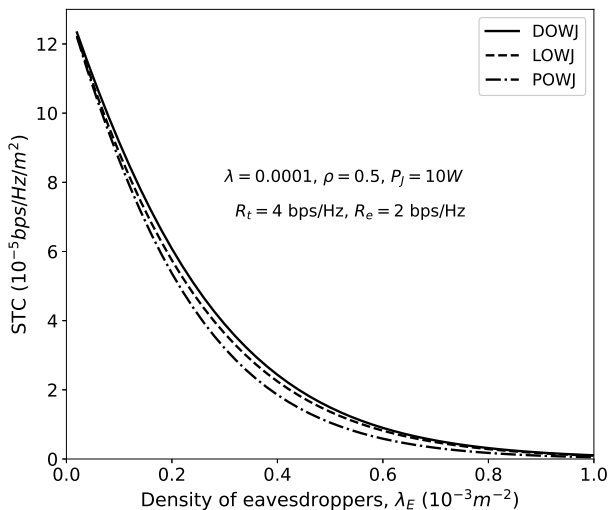
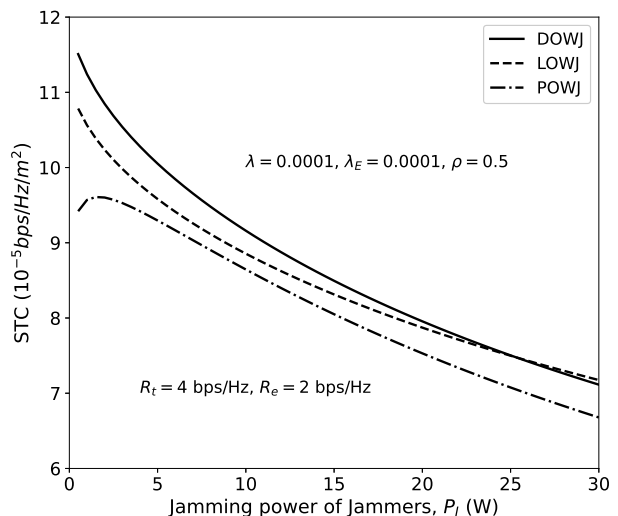
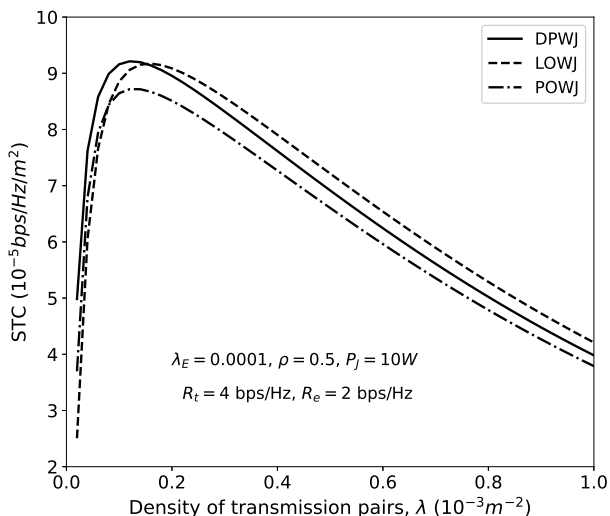
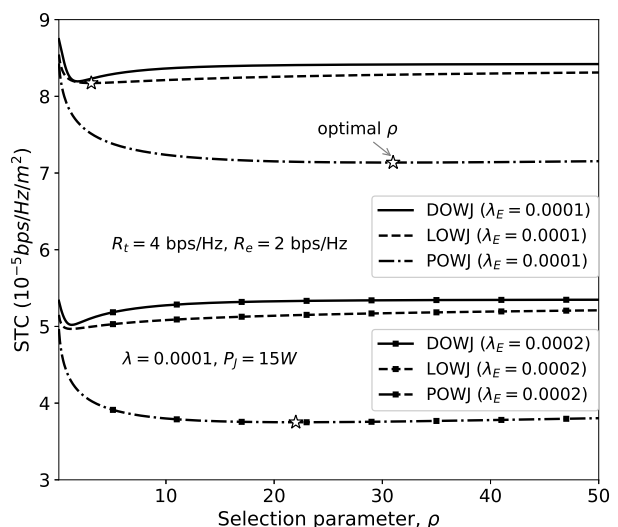
B. STC Performance Evaluation

1) *STC vs. λ_E* : We first explore the impact of the eavesdropper density λ_E on the network STC performance, for which we show in Fig. 3 STC vs. λ_E under all the three OWJ attacks for the settings of $\lambda = 0.0001$, $\rho = 0.5$, $P_J = 10$ W, $R_t = 4$ bps/Hz and $R_e = 2$ bps/Hz. The results show that the STC decreases as λ_E increases for a given ρ under all the three OWJ attacks, which is due to the more wiretappers and jammers resulting from the increased λ_E .

2) *STC vs. λ* : Next, we investigate how the density of transmission pairs (i.e., λ) affects the network STC performance. Fig. 4 plots the STC vs. λ under all the three OWJ attacks for the settings of $\lambda_E = 0.0001$, $\rho = 0.5$, $P_J = 10$ W, $R_t = 4$

bps/Hz and $R_e = 2$ bps/Hz. We can see from Fig. 4 that, as λ increases, the STC first increases and then decreases under all three OWJ attacks. The reason is that the increase of λ dominates the trend of the STC for small λ 's, while as λ continues to increase, the secrecy probability remains almost unchanged and the decrease of the connection probability becomes the dominant factor, leading to the decrease of the STC. The results in Fig. 4 reveal the existence of the optimal density of transmission pairs given a network and its key parameters, which should be taken into consideration during the network design.

3) *STC vs. P_J* : We then investigate the impact of the jamming power P_J on the network STC performance in Fig. 5, which plots STC vs. P_J under all the three OWJ

Fig. 3. STC vs. eavesdropper density λ_E .Fig. 5. STC vs. jamming power P_J .Fig. 4. STC vs. transmission density λ .Fig. 6. STC vs. bias factor ρ under different settings of λ_E .

attacks for the settings of $\lambda = 0.0001$, $\lambda_E = 0.0001$, $\rho = 0.5$, $R_t = 4$ bps/Hz and $R_e = 2$ bps/Hz. We can observe from Fig. 5 that, as P_J increases, the STC under the DOWJ and LOWJ attacks decreases while that under the POWJ attack first increases and then decreases. This is because the selections of attack patterns in the DOWJ and LOWJ attacks are independent of P_J and thus the increase of P_J leads to only the increase of the interference level to the receivers, decreasing the connection probabilities. For the POWJ attack, as P_J increases, the probability of wiretapping decreases while that of jamming increases, leading to increased secrecy probability and decreased connection probability. The STC is dominated by the secrecy probability for small ρ 's and dominated by the connection probability for large ρ 's.

4) *STC vs. ρ* : We finally explore the impact of the bias factor ρ on the network STC performance under the three OWJ attacks. Fig. 6 shows the results of STC vs. ρ under the settings of $R_t = 4$ bps/Hz, $R_e = 2$ bps/Hz, $\lambda = 0.0001$ and

$P_J = 15$ W. In addition, we consider two different settings of λ_E (i.e., $\lambda_E = 0.0001$ and $\lambda_E = 0.0002$). We can see from Fig. 6 that, as ρ increases, the STC first decreases and then increases under all the three OWJ attacks, implying the existence of the optimal ρ for eavesdroppers to minimize the network STC performance, i.e., maximizing the attack effect. This shows that neither pure jamming (i.e., $\rho \rightarrow 0$) nor pure wiretapping (i.e., $\rho \rightarrow \infty$) is the optimal strategy and the OWJ attacks are more favorable for eavesdroppers.

Careful observation shows that the optimal ρ decreases as λ_E increases, indicating that eavesdroppers prefer the jamming attack more as their density increases. To compare the attack effect of the three OWJ attacks, we focus on the worst STC performance they can achieve. Fig. 6 shows that the worst STC achieved by the POWJ attack is the smallest among the three OWJ attacks, which implies that the POWJ attack represents the most hazardous attack and the information of effective antenna gain plays a significant role in improving the attack

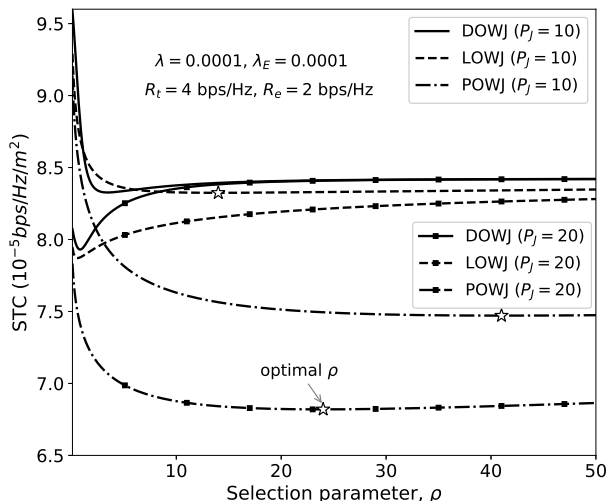


Fig. 7. STC vs. bias factor ρ under different settings of P_J .

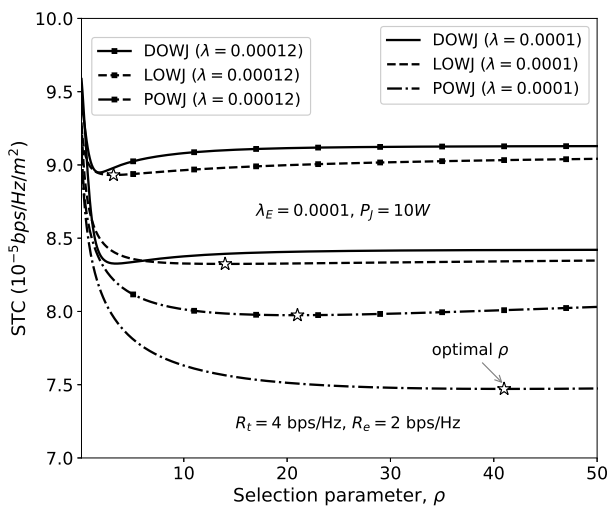


Fig. 8. STC vs. bias factor ρ under different settings of λ .

effect. We can also see that the worst STC achieved by the LOWJ attack is almost the same as that achieved by the DOWJ attack, which indicates that the information of link status has little impact on improving the attack effect.

To show the generality of our findings, we also plot STC vs. ρ in Fig. 7 under the settings of $\lambda = 0.0001$, $\lambda_E = 0.0001$, $R_t = 4$ bps/Hz, $R_e = 2$ bps/Hz and two different jamming powers, i.e., $P_J = 10$ W and $P_J = 20$ W, and in Fig. 8 under the settings of $\lambda_E = 0.0001$, $R_t = 4$ bps/Hz, $R_e = 2$ bps/Hz, $P_J = 10$ W and two different densities of transmission pairs, i.e., $\lambda = 0.0001$ and $\lambda = 0.00012$. Findings similar to those in Fig. 6 can be observed from both figures. We can also see from Fig. 7 and Fig. 8 that the optimal ρ decreases as the jamming power P_J and the transmission density λ increase, respectively, suggesting that eavesdroppers prefer the jamming attack more if they can choose a larger jamming power, or when more transmissions exist in the network.

VII. CONCLUSIONS

This paper proposed a new opportunistic wiretapping and jamming (OWJ) attack model for millimeter-wave (mmWave) wireless networks and provided three realizations, namely DOWJ, LOWJ and POWJ, each with a different cost model. Analytical expressions of secrecy transmission capacity (STC) were also derived to depict the network security performance under the OWJ attack. The results showed that the OWJ attack model causes more significant network security performance degradation than the pure wiretapping or jamming attack. In addition, POWJ is the most hazardous, while DOWJ and LOWJ achieve almost the same attack effect. This reveals that the effective antenna gain can be exploited to significantly improve the attack effect, whereas the link status has little impact on the improvement.

APPENDIX A PROOF OF LEMMA 2

Suppose $d_{x_0,z} = u$. We define $\tilde{D}_W^z = \min_{x \in \Phi_T \setminus \{x_0\}} d_{x,z}$ and $\tilde{D}_J^z = \min_{y \in \Phi_R \setminus \{y_0\}} d_{y,z}$. The event $\mathbf{1}_J^z = 1$ occurs in the following cases:

- x_0 is the nearest transmitter to z (i.e., $\tilde{D}_W^z \geq u$), y_0 is the nearest receiver to z (i.e., $\tilde{D}_J^z \geq v$) and $u \geq \rho v$;
- x_0 is the nearest transmitter to z (i.e., $\tilde{D}_W^z \geq u$), y_0 is *not* the nearest receiver to z (i.e., $\tilde{D}_J^z < v$) and $u \geq \rho \tilde{D}_J^z$;
- x_0 is *not* the nearest transmitter to z (i.e., $\tilde{D}_W^z < u$), y_0 is the nearest receiver to z (i.e., $\tilde{D}_J^z \geq v$) and $\tilde{D}_W^z \geq \rho v$;
- x_0 is *not* the nearest transmitter to z (i.e., $\tilde{D}_W^z < u$), y_0 is *not* the nearest receiver to z (i.e., $\tilde{D}_J^z < v$) and $\tilde{D}_W^z \geq \rho \tilde{D}_J^z$.

Combining the four cases, we have $\mathbf{1}_J^z = 1$ if

$$\begin{cases} \tilde{D}_W^z \geq \rho \tilde{D}_J^z, \tilde{D}_J^z < \frac{u}{\rho}, & u < \rho v, \\ \tilde{D}_W^z \geq \rho v, \tilde{D}_J^z \geq v \text{ or } \tilde{D}_W^z \geq \rho \tilde{D}_J^z, \tilde{D}_J^z < v, & u \geq \rho v. \end{cases} \quad (51)$$

Note that \tilde{D}_W^z (resp. \tilde{D}_J^z) has the same PDF and CDF as those of D_W^z (resp. D_J^z). With the help of the PDFs and CCDFs of D_W^z and D_J^z , we obtain the probability of $\mathbf{1}_J^z = 1$ conditioned on $d_{x_0,z} = u$ as follows:

$$\zeta(u, v) = \begin{cases} \frac{1}{\rho^2 + 1} (1 - e^{-(1 + \frac{1}{\rho^2}) \lambda \pi u^2}), & u < \rho v \\ \frac{1}{\rho^2 + 1} + \frac{\rho^2}{\rho^2 + 1} e^{-(\rho^2 + 1) \lambda \pi v^2}, & u \geq \rho v \end{cases} \quad (52)$$

From [27], we know that the CCDF and PDF of $d_{x_0,z}$ can be given by (14) and (15), respectively. Calculating the expectation of (52) in terms of $d_{x_0,z}$ yields $\zeta(v)$ in (13).

APPENDIX B PROOF OF LEMMA 4

Similar to the proof of Lemma 2 in Appendix A, we first derive the probability of $\mathbf{1}_J^z = 1$ (denoted by $\zeta_K^T(u, v)$) given the distance $d_{x_0,z}$ and status $\mathcal{S}_{x_0,z}$ of the link $x_0 \rightarrow z$. Suppose

$d_{x_0,z} = u$ and $\mathcal{S}_{x_0,z} = \kappa \in \{L, N\}$. It follows from Appendix A that $\mathbf{1}_J^z = 1$ if

$$\begin{cases} \tilde{\mathbf{L}}_T^z \geq \rho \tilde{\mathbf{L}}_R^z, \tilde{\mathbf{L}}_R^z < \frac{u^{\alpha_\kappa}}{\rho}, & u^{\alpha_\kappa} < \rho v^{\alpha_\tau}, \\ \tilde{\mathbf{L}}_T^z \geq \rho v^{\alpha_\tau}, \tilde{\mathbf{L}}_R^z \geq v^{\alpha_\tau} \text{ or } \tilde{\mathbf{L}}_T^z \geq \rho \tilde{\mathbf{L}}_R^z, \tilde{\mathbf{L}}_R^z < v^{\alpha_\tau}, & u^{\alpha_\kappa} \geq \rho v^{\alpha_\tau}, \end{cases} \quad (53)$$

where $\tilde{\mathbf{L}}_T^z = \min_{x \in \Phi_T \setminus \{x_0\}} d_{y,z}^\alpha$ and $\tilde{\mathbf{L}}_R^z = \min_{x \in \Phi_R \setminus \{y_0\}} d_{y,z}^\alpha$. Next, we need to derive the PDFs and CCDFs of $\tilde{\mathbf{L}}_T^z$ and $\tilde{\mathbf{L}}_R^z$. The CCDF of $\tilde{\mathbf{L}}_T^z$ is

$$\begin{aligned} \mathbb{P}(\tilde{\mathbf{L}}_T^z > w) &= \mathbb{P}\left(\min_{x \in \Phi_T \setminus \{x_0\}} d_{x,z}^\alpha > w\right) \\ &= \mathbb{P}\left(\bigcap_{x \in \Phi_T \setminus \{x_0\}} \{d_{x,z}^\alpha > w\}\right) \\ &= \mathbb{E}_{\Phi_T} \left[\prod_{x \in \Phi_T \setminus \{x_0\}} \mathbb{P}(d_{x,z}^\alpha > w) \right] \\ &= \exp\left(-2\pi\lambda \int_0^\infty (1 - \mathbb{P}(r^\alpha > w)) r dr\right) \\ &\stackrel{(b)}{=} e^{-\Lambda(\lambda, w)}, \end{aligned} \quad (54)$$

where (b) follows after changing $\mathbb{P}(r^\alpha > w)$ to $p_L(r)\mathbf{1}_{r^{\alpha_L} > w} + p_N(r)\mathbf{1}_{r^{\alpha_N} > w}$. Note that the CCDF of $\tilde{\mathbf{L}}_R^z$ is identical to that of $\tilde{\mathbf{L}}_T^z$. Hence, the PDF of $\tilde{\mathbf{L}}_R^z$ is

$$f_{\tilde{\mathbf{L}}_R^z}(w) = e^{-\Lambda(\lambda, w)} \Lambda'(\lambda, w). \quad (55)$$

Thus, for $u^{\alpha_\kappa} < \rho v^{\alpha_\tau}$, the probability of $\mathbf{1}_J^z = 1$ is

$$\begin{aligned} \zeta_\kappa^\tau(u, v) &= \int_0^{\frac{u^{\alpha_\kappa}}{\rho}} \mathbb{P}(\tilde{\mathbf{L}}_T^z \geq \rho w) f_{\tilde{\mathbf{L}}_R^z}(w) dw \\ &= \int_0^{\frac{u^{\alpha_\kappa}}{\rho}} e^{-(\Lambda(\lambda, \rho w) + \Lambda(\lambda, w))} \Lambda'(\lambda, w) dw. \end{aligned} \quad (56)$$

For $u^{\alpha_\kappa} \geq \rho v^{\alpha_\tau}$, the probability is

$$\begin{aligned} \zeta_\kappa^\tau(u, v) &= \mathbb{P}(\tilde{\mathbf{L}}_T^z \geq \rho v^{\alpha_\tau}, \tilde{\mathbf{L}}_R^z \geq v^{\alpha_\tau}) \\ &\quad + \mathbb{P}(\tilde{\mathbf{L}}_T^z \geq \rho \tilde{\mathbf{L}}_R^z, \tilde{\mathbf{L}}_R^z < v^{\alpha_\tau}) \\ &= e^{-(\Lambda(\lambda, \rho v^{\alpha_\tau}) + \Lambda(\lambda, v^{\alpha_\tau}))} \\ &\quad + \int_0^{v^{\alpha_\tau}} e^{-(\Lambda(\lambda, \rho w) + \Lambda(\lambda, w))} \Lambda'(\lambda, w) dw \\ &= 1 - \rho \int_0^{v^{\alpha_\tau}} e^{-(\Lambda(\lambda, \rho w) + \Lambda(\lambda, w))} \Lambda'(\lambda, \rho w) dw. \end{aligned} \quad (57)$$

Finally, taking the expectation of $\zeta_\kappa^\tau(u, v)$ in terms of $d_{x_0,z}$ and $\mathcal{S}_{x_0,z}$ completes the proof.

APPENDIX C PROOF OF LEMMA 6

Following the idea in Appendix B, we first derive the probability of $\mathbf{1}_J^z = 1$ (denoted by $\zeta_{\kappa,l,m}^{\tau,n,o}(u, v)$) conditioned on $d_{x_0,z} = u$, status $\mathcal{S}_{x_0,z} = \kappa$, effective antenna gain $\mathbf{G}_{T,W}^{x_0,z} = G_l^T G_m^W$ of the link $x_0 \rightarrow z$. From Appendix A, we can see that $\mathbf{1}_J^z = 1$ if

$$\begin{cases} \tilde{\mathbf{P}}_T^z \geq \rho \tilde{\mathbf{P}}_R^z, \tilde{\mathbf{P}}_R^z < \frac{\eta_1}{\rho}, & \eta_1 < \rho \eta_2, \\ \tilde{\mathbf{P}}_T^z \geq \rho \eta_2, \tilde{\mathbf{P}}_R^z \geq \eta_2 \text{ or } \tilde{\mathbf{P}}_T^z \geq \rho \tilde{\mathbf{P}}_R^z, \tilde{\mathbf{P}}_R^z < \eta_2, & \eta_1 \geq \rho \eta_2, \end{cases} \quad (58)$$

where $\tilde{\mathbf{P}}_T^z = \min_{x \in \Phi_T \setminus \{x_0\}} d_{x,z}^\alpha / (P_T \mathbf{G}_{T,W})$ and $\tilde{\mathbf{L}}_R^z = \min_{x \in \Phi_R \setminus \{y_0\}} d_{y,z}^\alpha / (P_J \mathbf{G}_{J,R})$.

Letting $\tilde{\mathbf{L}}_T^{z,i,j} = \min_{x \in \Phi_T^{i,j} \setminus \{x_0\}} d_{x,z}^\alpha$, where $\Phi_T^{i,j}$ is the PPP of transmitters with antenna gain $G_i^T G_j^W$ to z , we have

$$\begin{aligned} \mathbb{P}(\tilde{\mathbf{P}}_T^z > w) &= \prod_{i,j} \mathbb{P}\left(\tilde{\mathbf{L}}_T^{z,i,j} > w P_T G_i^T G_j^W\right) \\ &\stackrel{(c)}{=} \prod_{i,j} e^{-\Lambda(p_{ij}^{TW} \lambda, P_T G_i^T G_j^W w)} \\ &= \exp\left(-\sum_{i,j} \Lambda(p_{ij}^{TW} \lambda, P_T G_i^T G_j^W w)\right) \\ &= e^{-\hat{\Lambda}_1(\lambda, w)}, \end{aligned} \quad (59)$$

where $i \in \{M, S\}$, $j \in \{M, S\}$ and (c) follows from (54). Similarly, we have

$$\mathbb{P}(\tilde{\mathbf{P}}_R^z > w) = e^{-\hat{\Lambda}_2(\lambda, w)}. \quad (60)$$

The PDFs of $\tilde{\mathbf{P}}_T^z$ and $\tilde{\mathbf{P}}_R^z$ can be derived accordingly. Based on the PDFs and CCDFs of $\tilde{\mathbf{P}}_T^z$ and $\tilde{\mathbf{P}}_R^z$, we can obtain the probability $\zeta_{\kappa,l,m}^{\tau,n,o}(u, v)$ as in (28) and (29). Finally, neglecting the dependence between $\mathbf{G}_{T,W}^{x_0,z}$ and $\mathbf{G}_{J,R}^{z,y_0}$ and taking the expectation of $\zeta_{\kappa,l,m}^{\tau,n,o}(u, v)$ in terms of $d_{x_0,z}$, $\mathcal{S}_{x_0,z}$ and $\mathbf{G}_{T,W}^{x_0,z}$, we complete the proof.

APPENDIX D PROOF OF LEMMA 8

We first calculate the Laplace transform of \hat{I}_z^T conditioned on $d_{y_0,z} = v$, which is given by

$$\begin{aligned} \mathcal{L}_z^T(s, u, v) &= \mathbb{E}[e^{-s \hat{I}_z^T}] \\ &= \mathbb{E}[e^{-s \hat{I}_z^T} | \mathbf{1}_J^z = 1] \mathbb{P}(\mathbf{1}_J^z = 1) \\ &\quad + \mathbb{E}[e^{-s \hat{I}_z^T} | \mathbf{1}_J^z = 0] \mathbb{P}(\mathbf{1}_J^z = 0) \\ &= \mathbb{E}[e^{-s \hat{I}_z^T} | \mathbf{1}_J^z = 0] \mathbb{P}(\mathbf{1}_J^z = 0) \\ &= \mathbb{E}[e^{-s \hat{I}_z^T}] - \mathbb{E}[e^{-s \hat{I}_z^T} | \mathbf{1}_J^z = 1] \mathbb{P}(\mathbf{1}_J^z = 1). \end{aligned} \quad (61)$$

Following from Lemma 1, $\mathbb{E}[e^{-s \hat{I}_z^T}]$ can be given by

$$\mathbb{E}[e^{-s \hat{I}_z^T}] = \Xi_{T,W}[s, \lambda, 0]. \quad (62)$$

According to the conditions of $\mathbf{1}_J^z = 1$ in (51), we have

$$\begin{aligned} \mathcal{L}_z^T(s, u, v) &= \mathbb{E}[e^{-s \hat{I}_z^T}] \\ &\quad - \int_0^{\frac{u}{\rho}} \mathbb{E}[e^{-s \hat{I}_z^T} | \tilde{\mathbf{D}}_T^z \geq \rho w] \mathbb{P}(\tilde{\mathbf{D}}_T^z \geq \rho w) f_{\tilde{\mathbf{D}}_R^z}(w) dw \\ &= \Xi_{T,W}(s, \lambda, 0) \\ &\quad - \int_0^{\frac{u}{\rho}} \Xi_{T,W}(s, \lambda, \rho w) 2\pi \lambda w e^{-(\rho^2+1)\lambda\pi w^2} dw \end{aligned} \quad (63)$$

for $u < \rho v$, and

$$\begin{aligned} \mathcal{L}_z^T(s, u, v) &= \mathbb{E}[e^{-s \hat{I}_z^T}] \\ &\quad - \mathbb{E}[e^{-s \hat{I}_z^T} | \tilde{\mathbf{D}}_T^z \geq \rho v] \mathbb{P}(\tilde{\mathbf{D}}_T^z \geq \rho v) \mathbb{P}(\tilde{\mathbf{D}}_R^z \geq v) \\ &\quad - \int_0^v \mathbb{E}[e^{-s \hat{I}_z^T} | \tilde{\mathbf{D}}_T^z \geq \rho w] \mathbb{P}(\tilde{\mathbf{D}}_T^z \geq \rho w) f_{\tilde{\mathbf{D}}_R^z}(w) dw \\ &= \Xi_{T,W}(s, \lambda, 0) - e^{-(\rho^2+1)\lambda\pi v^2} \Xi_{T,W}(s, \lambda, \rho v) \\ &\quad - \int_0^v \Xi_{T,W}(s, \lambda, \rho w) 2\pi \lambda w e^{-(\rho^2+1)\lambda\pi w^2} dw \end{aligned} \quad (64)$$

for $u \geq \rho v$. Taking the expectation of $\mathcal{L}_z^T(s, u, v)$ in terms of $d_{y_0, z}$ completes the proof.

APPENDIX E
PROOF OF LEMMA 9

We first calculate the Laplace transform conditioned on $d_{y_0, z} = v$ and $\mathcal{S}_{y_0, z} = \tau$ (denoted by $\mathcal{L}_{z, \kappa}^{T, \tau}(s, u, v)$). According to (61), we need to derive $\mathbb{E}[e^{-sI_z^T} | \mathbf{1}_j^z = 1] \mathbb{P}(\mathbf{1}_j^z = 1)$. We rewrite I_z^T as

$$I_z^T = \sum_{k \in \{L, N\}} I_z^{T, k}, \quad (65)$$

where $I_z^{T, k} = \sum_{x \in \Phi_T^k \setminus \{x_0\}} P_T G_{T, W}^{x, z} h_{x, z} d_{x, z}^{-\alpha}$ denotes the interference from the sub-PPP Φ_T^k of transmitters with link status k to z .

Defining $\tilde{D}_{T, k}^z = \min_{x \in \Phi_T^k \setminus \{x_0\}} d_{x, z}$, we have

$$\begin{aligned} \mathcal{L}_{z, \kappa}^{T, \tau}(s, u, v) &= \mathbb{E}[e^{-sI_z^T}] - \int_0^{\frac{u\alpha\kappa}{\rho}} \mathbb{P}(\tilde{L}_T^z \geq \rho w) f_{\tilde{L}_R^z}(w) \quad (66) \\ &\quad \prod_k \mathbb{E}[e^{-sI_z^{T, k}} | \tilde{L}_T^z \geq \rho w] dw \\ &= \mathbb{E}[e^{-sI_z^T}] - \int_0^{\frac{u\alpha\kappa}{\rho}} \mathbb{P}(\tilde{L}_T^z \geq \rho w) f_{\tilde{L}_R^z}(w) \\ &\quad \prod_k \mathbb{E}[e^{-sI_z^{T, k}} | \tilde{D}_{T, k}^z \geq (\rho w)^{\frac{1}{\alpha_k}}] dw \end{aligned}$$

for $u\alpha\kappa < \rho v^{\alpha\tau}$, and

$$\begin{aligned} \mathcal{L}_{z, \kappa}^{T, \tau}(s, u, v) &= \mathbb{E}[e^{-sI_z^T}] - \mathbb{E}[e^{-sI_z^T} | \tilde{L}_T^z \geq \rho v^{\alpha\tau}] \quad (67) \\ &\quad \times \mathbb{P}(\tilde{L}_T^z \geq \rho v^{\alpha\tau}, \tilde{L}_R^z \geq v^{\alpha\tau}) \\ &\quad - \int_0^{\rho v^{\alpha\tau}} \mathbb{P}(\tilde{L}_T^z \geq \rho w) f_{\tilde{L}_R^z}(w) \\ &\quad \prod_k \mathbb{E}[e^{-sI_z^{T, k}} | \tilde{D}_{T, k}^z \geq (\rho w)^{\frac{1}{\alpha_k}}] dw \end{aligned}$$

for $u\alpha\kappa \geq \rho v^{\alpha\tau}$. After some mathematical manipulations based on (63) and (64), we obtain the expression of $\mathcal{L}_{z, \kappa}^{T, \tau}(s, u, v)$ in (47). We complete the proof after calculating the expectation of $\mathcal{L}_{z, \kappa}^{T, \tau}(s, u, v)$ in terms of $d_{y_0, z}$ and $\mathcal{S}_{y_0, z}$.

APPENDIX F
PROOF OF LEMMA 10

Similar to Appendix E, we first derive the Laplace transform conditioned on $d_{y_0, z} = v$, $\mathcal{S}_{y_0, z} = \tau$ and $\mathbf{G}_{J, R}^{z, y_0} = G_n^J G_o^R$ (denoted by $\mathcal{L}_{z, \kappa, l, m}^{T, \tau, n, o}(s, u, v)$). We rewrite I_z^T as

$$I_z^T = \sum_{k \in \{L, N\}} \sum_{i \in \{M, S\}} \sum_{j \in \{M, S\}} I_z^{T, k, i, j}, \quad (68)$$

where $I_z^{T, k, i, j} = \sum_{x \in \Phi_T^{k, i, j} \setminus \{x_0\}} P_T G_{T, W}^{x, z} h_{x, z} d_{x, z}^{-\alpha}$ denotes the interference from the sub-PPP $\Phi_T^{k, i, j}$ of transmitters with link status k and channel gain $G_i^T G_j^W$ to z .

Let $\tilde{D}_{T, k, i, j}^z = \min_{x \in \tilde{\Phi}_{T, k, i, j}^z \setminus \{x_0\}} d_{x, z}$. According to (58), for $\eta_1 < \rho\eta_2$, the Laplace transform $\mathcal{L}_{z, \kappa, l, m}^{T, \tau, n, o}(s, u, v)$ is

$$\begin{aligned} \mathbb{E}[e^{-sI_z^T}] &- \int_0^{\frac{\eta_1}{\rho}} \mathbb{P}(\tilde{P}_T^z \geq \rho w) f_{\tilde{P}_R^z}(w) \quad (69) \\ &\quad \times \prod_{k, i, j} \mathbb{E}[e^{-sI_z^{T, k, i, j}} | \tilde{D}_{T, k, i, j}^z \geq (\rho w P_T G_i^T G_j^W)^{\frac{1}{\alpha_k}}] dw. \end{aligned}$$

For $\eta_1 \geq \rho\eta_2$, the Laplace transform $\mathcal{L}_{z, \kappa, l, m}^{T, \tau, n, o}(s, u, v)$ is

$$\begin{aligned} \mathbb{E}[e^{-sI_z^T}] &- \mathbb{E}[e^{-sI_z^T} | \tilde{P}_T^z \geq \rho\eta_2] \mathbb{P}(\tilde{P}_T^z \geq \rho\eta_2, \tilde{P}_R^z \geq \eta_2) \\ &- \int_0^{\eta_2} \mathbb{P}(\tilde{P}_T^z \geq \rho w) f_{\tilde{P}_R^z}(w) \\ &\quad \times \prod_{k, i, j} \mathbb{E}[e^{-sI_z^{T, k, i, j}} | \tilde{D}_{T, k, i, j}^z \geq (\rho w P_T G_i^T G_j^W)^{\frac{1}{\alpha_k}}] dw. \quad (70) \end{aligned}$$

We then obtain the expression of $\mathcal{L}_{z, \kappa, l, m}^{T, \tau, n, o}(s, u, v)$ in (48) after conducting some mathematical manipulations. Calculating the expectation of $\mathcal{L}_{z, \kappa, l, m}^{T, \tau, n, o}(s, u, v)$ in terms of $d_{y_0, z}$, $\mathcal{S}_{y_0, z}$ and $\mathbf{G}_{J, R}^{z, y_0}$ completes the proof.

REFERENCES

- [1] T. S. Rappaport, S. Sun, R. Mayzus, H. Zhao, Y. Azar, K. Wang, G. N. Wong, J. K. Schulz, M. Samimi, and F. Gutierrez, "Millimeter wave mobile communications for 5g cellular: It will work!" *IEEE Access*, vol. 1, pp. 335–349, 2013.
- [2] S. Rangan, T. S. Rappaport, and E. Erkip, "Millimeter-wave cellular wireless networks: Potentials and challenges," *Proceedings of the IEEE*, vol. 102, no. 3, pp. 366–385, 2014.
- [3] W. Hong, Z. H. Jiang, C. Yu, D. Hou, H. Wang, C. Guo, Y. Hu, L. Kuai, Y. Yu, Z. Jiang, Z. Chen, J. Chen, Z. Yu, J. Zhai, N. Zhang, L. Tian, F. Wu, G. Yang, Z.-C. Hao, and J. Y. Zhou, "The role of millimeter-wave technologies in 5g/6g wireless communications," *IEEE J. Microwaves*, vol. 1, no. 1, pp. 101–122, 2021.
- [4] Z. Xiao, L. Zhu, Y. Liu, P. Yi, R. Zhang, X.-G. Xia, and R. Schober, "A survey on millimeter-wave beamforming enabled uav communications and networking," *IEEE Commun. Surveys Tuts.*, vol. 24, no. 1, pp. 557–610, 2022.
- [5] Z.-J. Guo, Z.-C. Hao, H.-Y. Yin, D.-M. Sun, and G. Q. Luo, "Planar shared-aperture array antenna with a high isolation for millimeter-wave low earth orbit satellite communication system," *IEEE Trans. Antennas Propag.*, vol. 69, no. 11, pp. 7582–7592, 2021.
- [6] Y. Zhang, Y. Shen, X. Jiang, and S. Kasahara, "Mode selection and spectrum partition for d2d inband communications: A physical layer security perspective," *IEEE Trans. Commun.*, vol. 67, no. 1, pp. 623–638, Jan 2019.
- [7] S. Zhao, J. Liu, Y. Shen, X. Jiang, and N. Shiratori, "Secure and energy-efficient precoding for mimo two-way untrusted relay systems," *IEEE Trans. Inf. Forensics Security*, vol. 16, pp. 3371–3386, 2021.
- [8] Y. Xu, J. Liu, Y. Shen, X. Jiang, Y. Ji, and N. Shiratori, "Qos-aware secure routing design for wireless networks with selfish jammers," *IEEE Transactions on Wireless Communications*, vol. 20, no. 8, pp. 4902–4916, 2021.
- [9] S. Zhao, J. Liu, Y. Shen, X. Jiang, and N. Shiratori, "Secure beamforming for full-duplex mimo two-way untrusted relay systems," *IEEE Trans. Inf. Forensics Security*, vol. 15, pp. 3775–3790, 2020.
- [10] J. He, J. Liu, Y. Shen, X. Jiang, and N. Shiratori, "Link selection for security-qos tradeoffs in buffer-aided relaying networks," *IEEE Trans. Inf. Forensics Security*, vol. 15, pp. 1347–1362, 2020.
- [11] Z. Kong, J. Song, C. Wang, H. Chen, and L. Hanzo, "Hybrid analog-digital precoder design for securing cognitive millimeter wave networks," *IEEE Trans. Inf. Forensics Security*, vol. 16, pp. 4019–4034, 2021.
- [12] J. Xu, W. Xu, D. W. K. Ng, and A. L. Swindlehurst, "Secure communication for spatially sparse millimeter-wave massive mimo channels via hybrid precoding," *IEEE Trans. Commun.*, vol. 68, no. 2, pp. 887–901, 2020.

- [13] K. Wu, W. Ni, J. A. Zhang, R. P. Liu, and J. Guo, "Secrecy rate analysis for millimeter-wave lens antenna array transmission," *IEEE Commun. Lett.*, vol. 24, no. 2, pp. 272–276, 2020.
- [14] W. Hao, G. Sun, J. Zhang, P. Xiao, and L. Hanzo, "Secure millimeter wave cloud radio access networks relying on microwave multicast fronthaul," *IEEE Trans. Commun.*, vol. 68, no. 5, pp. 3079–3095, 2020.
- [15] J. Song, B. Lee, J. Park, M.-S. Lee, and J.-H. Lee, "Beamformer design for physical layer security in dual-polarized millimeter wave channels," *IEEE Trans. Veh. Technol.*, vol. 69, no. 10, pp. 12 306–12 311, 2020.
- [16] S. Huang, M. Xiao, and H. V. Poor, "On the physical layer security of millimeter wave noma networks," *IEEE Trans. Veh. Technol.*, vol. 69, no. 10, pp. 11 697–11 711, 2020.
- [17] Y. Song, W. Yang, Z. Xiang, H. Wang, and F. Cao, "Research on cognitive power allocation for secure millimeter-wave noma networks," *IEEE Trans. Veh. Technol.*, vol. 69, no. 11, pp. 13 424–13 436, 2020.
- [18] Y. Yapici, N. Rupasinghe, I. Guvenc, H. Dai, and A. Bhuyan, "Physical layer security for noma transmission in mmwave drone networks," *IEEE Trans. Veh. Technol.*, vol. 70, no. 4, pp. 3568–3582, 2021.
- [19] X. Sun, W. Yang, and Y. Cai, "Secure communication in noma-assisted millimeter-wave swipt uav networks," *IEEE Internet of Things Journal*, vol. 7, no. 3, pp. 1884–1897, 2020.
- [20] Y. Zhu, G. Zheng, and K.-K. Wong, "Stochastic geometry analysis of large intelligent surface-assisted millimeter wave networks," *IEEE J. Sel. Areas Commun.*, vol. 38, no. 8, pp. 1749–1762, 2020.
- [21] C. Wang, Z. Li, T.-X. Zheng, D. W. K. Ng, and N. Al-Dhahir, "Intelligent reflecting surface-aided secure broadcasting in millimeter wave symbiotic radio networks," *IEEE Trans. Veh. Technol.*, vol. 70, no. 10, pp. 11 050–11 055, 2021.
- [22] Y. Xiu, J. Zhao, W. Sun, and Z. Zhang, "Secrecy rate maximization for reconfigurable intelligent surface aided millimeter wave system with low-resolution dacs," *IEEE Commun. Lett.*, vol. 25, no. 7, pp. 2166–2170, 2021.
- [23] W. M. R. Shakir and M.-S. Alouini, "Secrecy performance analysis of parallel fso/mm-wave system over unified fisher-snedecor channels," *IEEE Photonics Journal*, vol. 14, no. 2, pp. 1–13, 2022.
- [24] S. C. Tokgoz, S. Althunibat, S. L. Miller, and K. A. Qaraqe, "On the secrecy capacity of hybrid fso-mmwave wiretap channels," *IEEE Trans. Veh. Technol.*, vol. 71, no. 4, pp. 4073–4086, 2022.
- [25] S. C. Tokgoz, S. Althunibat, S. Yarkan, and K. A. Qaraqe, "Physical layer security of hybrid fso-mmwave communications in presence of correlated wiretap channels," in *Proc. IEEE ICC*, 2021, pp. 1–7.
- [26] M. J. Saber and S. Rajabi, "On secrecy performance of millimeter-wave rf-assisted fso communication systems," *IEEE Syst. J.*, vol. 15, no. 3, pp. 3781–3788, 2021.
- [27] Y. Zhang, Y. Shen, X. Jiang, and S. Kasahara, "Secure millimeter-wave ad hoc communications using physical layer security," *IEEE Trans. Inf. Forensics Security*, vol. 17, pp. 99–114, 2022.
- [28] Y. Zhu, L. Wang, K. Wong, and R. W. Heath, "Secure communications in millimeter wave ad hoc networks," *IEEE Trans. Wireless Commun.*, vol. 16, no. 5, pp. 3205–3217, 2017.
- [29] Y. Zhu, G. Zheng, and M. Fitch, "Secrecy rate analysis of uav-enabled mmwave networks using matern hardcore point processes," *IEEE J. Sel. Areas Commun.*, vol. 36, no. 7, pp. 1397–1409, 2018.
- [30] T. S. Rappaport, Y. Xing, G. R. MacCartney, A. F. Molisch, E. Mellios, and J. Zhang, "Overview of millimeter wave communications for fifth-generation (5g) wireless networks—with a focus on propagation models," *IEEE Trans. Antennas Propag.*, vol. 65, no. 12, pp. 6213–6230, 2017.
- [31] J. Ma, R. Shrestha, J. Adelberg, C.-Y. Yeh, Z. Hossain, E. Knightly, J. M. Jornet, and D. M. Mittleman, "Security and eavesdropping in terahertz wireless links," *Nature*, vol. 563, no. 7729, pp. 89–93, 2018.
- [32] I. F. Akyildiz, J. M. Jornet, and C. Han, "Terahertz band: Next frontier for wireless communications," *Physical communication*, vol. 12, pp. 16–32, 2014.
- [33] J. F. Harvey, M. B. Steer, and T. S. Rappaport, "Exploiting high millimeter wave bands for military communications, applications, and design," *IEEE Access*, vol. 7, pp. 52 350–52 359, 2019.
- [34] Y. Zhang, J. He, Q. Qu, and Z. Zhang, "Wiretapping or jamming: On eavesdropper attacking strategy in mmwave ad hoc networks," in *Proc. IEEE NaNA*, 2021, pp. 8–14.
- [35] M. Haenggi, *Stochastic geometry for wireless networks*. Cambridge University Press, 2012.
- [36] A. Thornburg, T. Bai, and R. W. Heath, "Performance analysis of outdoor mmwave ad hoc networks," *IEEE Trans. Signal Process.*, vol. 64, no. 15, pp. 4065–4079, 2016.